Ozonolysis of Oleic Acid Adsorbed to Polar and Nonpolar Aerosol Particles

Elias P. Rosen, Eva R. Garland, and Tomas Baer*

Department of Chemistry, University of North Carolina, Chapel Hill, North Carolina 27599-3290

Received: May 23, 2008; Revised Manuscript Received: July 30, 2008

Single-particle kinetic studies of the reaction between oleic acid and O_3 have been conducted on two different types of core particles: polystyrene latex (PSL) and silica. Oleic acid was found to adsorb to both particle types in multilayer islands that resulted in an adsorbed layer of a total volume estimated to be less than one monolayer. The rate of the surface reaction between surface-adsorbed oleic acid and O_3 has been shown for the first time to be influenced by the composition of the aerosol substrate in a mixed organic/inorganic particle. A Langmuir−Hinshelwood mechanism was applied to the observed dependence of the pseudo-first-order rate constant with [O_3], and the resulting fit parameters for the ozone partition coefficient (K_{O_3}) and maximum first order rate constant ($k_{1,max}$) suggest that the reaction proceeded faster on the less polar PSL core at lower [O_3] due to the increased residence time of O_3 on the PSL surface, but the reaction was ultimately more efficient on the silica surface at high [O_3]. Values for the uptake coefficient, γ_{oleic}, for reaction of oleic acid on PSL spheres decrease from 2.5×10^{-5} to 1×10^{-5} with increasing [O_3] from 4 to 25 ppm and overlap at high [O_3] with the estimated values for γ_{oleic} on silica, which decrease from 1.6×10^{-5} to 1.3×10^{-5}. The relationship between γ_{oleic} and the more common expression for γ_{O_3} is discussed.

1. Introduction

Organic matter can comprise a significant portion of the atmospheric aerosol burden in both urban[1,2] and remote[3,4] settings. Chemical aging of organic aerosol particles by atmospheric oxidants changes their composition and reactivity, CCN ability, and optical properties, and can alter their effect on climate and human health. Processing of aerosols occurs through heterogeneous reactions between a gaseous oxidant and a condensed phase species that are controlled by many factors including gas phase diffusion, accommodation by the surface, and reaction either at the surface or within the bulk particle following diffusion.[5,6] Particle morphology plays an important role in influencing the reactivity once an oxidant comes into contact with an aerosol particle, as has become evident in the case of the reaction between oleic acid and ozone (O_3). Oleic acid is a monounsaturated fatty acid that is found in cooking oils and many types of meats and is the primary unsaturated species in olive oil. It is released to the atmosphere during meat cooking and has become a benchmark compound to study since it also serves as a suitable proxy for larger lipid systems. Oleic acid's double bond is susceptible to attack by O_3, and considerable experimental attention has been paid to the characterization of the products and kinetics of the reaction between oleic acid and O_3, which has been recently summarized in a comprehensive review.[7] Laboratory experiments measuring the rate of reaction of pure oleic acid and O_3 estimate a lifetime of oleic acid in the atmosphere on the order of seconds.[8−11] Yet, oleic acid persists in the atmosphere and has been collected in particulate form, suggesting a lifetime on the order of days.[3,12]

One obvious simplification in unary phase experiments is the homogeneity of pure oleic acid particles and films, and matrix effects within internally mixed ambient particles have long been hypothesized to be responsible for the difference in reactivity between unary phase and atmospheric oleic acid particles.[9,11] Subsequent laboratory studies have investigated the reactivity of oleic acid in internally mixed particles containing other organic acids expected to be released from meat cooking.[13−17] The phase and morphology of these mixed fatty acid systems vary widely and are dependent on the relative amounts of the components. These studies have demonstrated the important role of morphology in the reactivity of oleic acid particles, as well as some of the inherent difficulties associated with even an incremental increase in morphological complexity in kinetic studies. The particle morphology of the internally mixed fatty acid systems is highly dependent on the preparation of particles, which can undergo supercooling,[16] and the preparation of films, which can influence the resulting crystal structure.[15] When the resulting morphology involves oleic acid being encased or trapped by a diffusional barrier of a solid fatty acid, the reactive uptake coefficient of O_3 has been shown to decrease by more than an order of magnitude. While the reactivity of mixed fatty acid systems can be decreased relative to pure oleic acid based on the morphology, there still remains a gulf between laboratory measurements and field observations which indicates that the exploration of the reactivity involving different particle morphologies is warranted.

In addition to self-aggregating, organic species are frequently found to be internally mixed with inorganic particles of anthropogenic and biogenic origin that are prevalent in the atmosphere. Internal mixtures of organic material with sulfate, ammonium, sea salt, soot, and minerals have been measured.[1,4,18−23] Solid particles such as soot and dust represent a large fraction of the available surface area in the boundary layer on which low volatility organic species may condense, and the chemical composition of an aerosol core has been shown to affect the reactivity of an organic surfactant layer.[24−28]

Despite the potential atmospheric relevance, few studies have examined the kinetics of adsorbed oleic acid on solid inorganic particles. Katrib et al. coated oleic acid onto polystyrene latex spheres (PSLs) and monitored the change in aerodynamic diameter and density of the particle as it reacted with O_3 but did not report any kinetic information.[29] A recent study by

* Corresponding author. E-mail: baer@unc.edu. Phone:(919) 962-1580.

10.1021/jp8045802 CCC: $40.75
Published on Web 09/25/2008

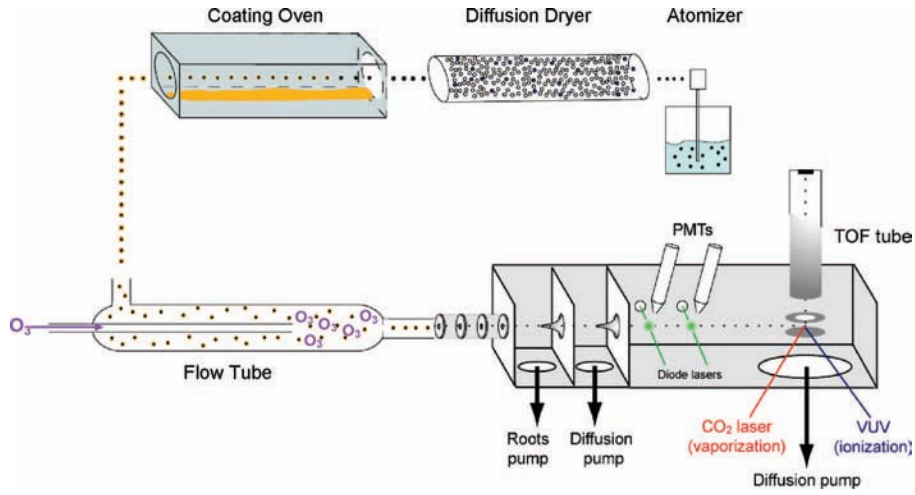

Figure 1. Experimental set-up: particle generation and coating, flow tube reactor, and particle characterization by ATOFMS.

McNeill et al. is the first to report kinetic information for a surfactant layer of sodium oleate on aqueous NaCl and Na_2SO_4 aerosols.[28] The goal of the present study was to investigate the reaction between oleic acid and O_3 on two different inorganic core particles: silica, which serves as an analogue to mineral dust; and polystyrene, which represents a hydrophobic surface like soot. The importance of size dependence and porosity of the core particles was also investigated. Flow tube studies employing single-particle mass spectrometry have been conducted to carefully measure the reaction kinetics of a surfactant layer of oleic acid on these two particle types.

2. Experimental Section

2.1. Generation of Coated Particles. Figure 1 shows the experimental setup used for particle generation and analysis. The core particles investigated were 1.6 and 3 μm PSLs (Duke Scientific), 1.6 μm silica spheres (Duke Scientific), and 3 μm highly porous silica spheres (Supelcosil, Supelco). Based on manufacturer's specifications, the Supelcosil spheres had pores of 12 nm in diameter resulting in a total particle surface area of approximately 1400 μm^2, which represents a 50-fold increase in total surface area over a solid sphere with a diameter of 3 μm. Equal concentrations of core particles were each suspended in a 50:50 water/methanol solution and aerosolized with filtered air using a constant output atomizer (TSI Inc., model 3076). The atomized particles passed through a heated tube followed by a diffusion dryer (TSI Inc., model 3062) to remove the solvent. The possibility of incomplete removal of adsorbed water on the core particle surface will be discussed later. The denuded core particles then entered a home-built oven for vapor deposition. The oven consisted of a 1.9 cm o.d., 33 cm long stainless steel tube encased in a solid aluminum block and contained a pool of liquid oleic acid along the length of the tube. Four cartridge heaters (Watlow, model C2A4) powered by a temperature controller (Watlow, Series 989) regulated the temperature of the oven and, in turn, the vapor pressure of the oleic acid. The range of oven temperatures explored (55−74 °C) corresponds to oleic acid vapor pressures between 1 and 6.5×10^{-3} Pa.[30]A laminar flow (Re = 35) of 1.3 standard liters per minute (SLM) through the oven provided a uniform contact of approximately 20 s between the core particles and the saturated vapor of oleic acid. Composition and morphology of the coated particles were evaluated with an aerosol time-of-flight mass spectrometer (ATOFMS), a scanning electron microscope (SEM), and an atomic force microscope (AFM). Particle sizing was performed by the ATOFMS and an aerodynamic particle sizer (APS; TSI Inc., model 3321).

2.2. Aerosol Flow Reactor Kinetics. Reaction between particle-bound oleic acid and O_3 was controlled in a flow tube and monitored with the ATOFMS. Details of the procedure have been presented elsewhere[10,13] and will be summarized here. All experiments were conducted at atmospheric pressure (1 atm), room temperature (298 K), and ambient humidity. The coated particle stream from the oven was introduced into a side port of a 2.54 cm i.d., 1 m long glass flow tube. The aerosol concentration in the flow tube was typically 10−100 particles cm^{-3} as measured by the APS, and there was no evidence for particle wall-loss in transit through the flow tube. O_3, produced by flowing O_2 through an ozone generator (Pacific Ozone Technology, model L11), was diluted by a factor of 45 with air before its concentration was determined by a 10 cm long home-built absorption cell monitoring the absorption of light at λ = 254 nm.[10] The O_3 flow was introduced into the flow tube through a 0.44 cm i.d. glass injector that could be moved over the length of the flow tube to vary the interaction time between the O_3 and the oleic acid. Velocity matching between the injected O_3 flow of 46 standard cubic centimeters per minute (sccm) and the aerosol flow ensured stable mixing and a laminar flow (Re = 18) through the flow tube. O_3 was held in excess of oleic acid by at least a factor of 35 such that its concentration was constant over the length of the flow tube, and the bimolecular ozonolysis reaction can be considered pseudo-first-order. No direct measurement of oleic acid deposition on the flow tube walls was made. However, since APS measurements did not indicate a change in particle concentration through the flow tube, any deposition would likely arise from any residual oleic acid vapor that did not condense onto the particles in the condensation oven and tubing prior to the flow tube. No difference in the ozonolysis kinetics was observed for pure oleic acid particles generated by (1) homogeneous nucleation of liquid oleic acid in the condensing oven and (2) atomizing a solution of oleic acid and methanol. This suggests that any oleic acid vapor adhering to the flow tube walls did not represent a significant sink for O_3. Additionally, there was no change in kinetics observed over a wide range of aerosol concentrations, confirming that O_3 was in excess.

2.3. Characterization of Coated Aerosols. ***2.3.1. Online Measurement with Aerosol Time of Flight Mass Spectrometry.*** After traversing the flow tube, the particles entered the ATOFMS through an aerodynamic lens, which focused the

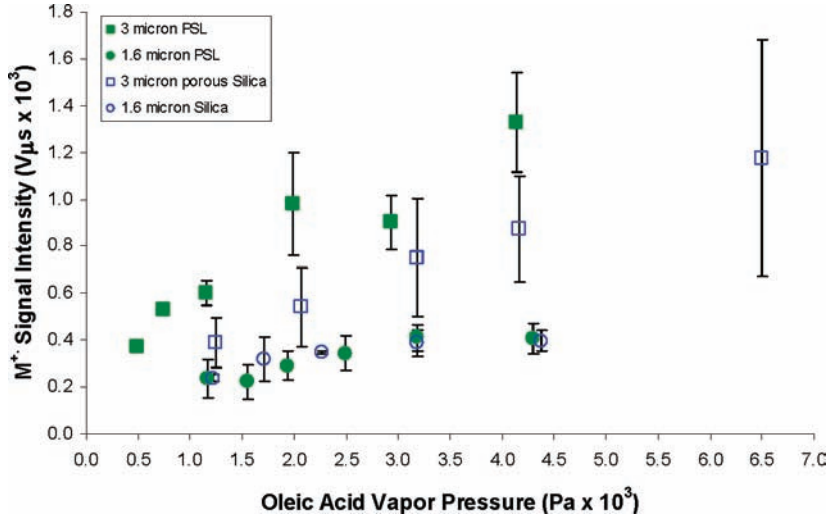

Figure 2. Optimized M+ ($m/z = 282$) signal intensity of adsorbed oleic acid plotted as a function of oleic acid vapor pressure in the coating oven for each core type and size. Error bars represent $\pm 1\sigma$.

particles into a narrow beam. The particles were accelerated proportionally to their size by the supersonic expansion of gases as the aerosol moved from the ambient conditions of the flow tube to the evacuated main chamber (10^{-7} Torr) of the ATOFMS. The particle trajectory through the chamber intersected the incident beams of two 532 nm green diode lasers separated by 10 cm. Light that was sequentially scattered by the particle as it passed through each beam was collected by separate photomultiplier tubes (PMTs) and translated into an electronic signal. A digital timing circuit used this signal to calculate each particle's velocity and coordinated the charging and firing of a two-step laser desorption/ionization process. Upon arrival in the center of the instrument, a particle was first volatilized by radiation from a CO_2 laser ($\lambda = 9.3-10\ \mu$m) and subsequently ionized by 118 nm vacuum UV light produced by frequency tripling the 355 nm output of a Nd/YAG laser in a Xe/Ar gas cell. Although this two-laser scheme has been shown to result in a greater degree of analyte fragmentation for liquid organic aerosols relative to desorption by a cartridge heater,[31] particle bounce off on the cartridge heater by the refractory solid core of the coated particles prevented surfactant detection. Prior to data collection, laser powers and temporal separation between IR and VUV firing were adjusted to maximize the intensity of the oleic acid molecular ion (M+, $m/z = 282$) peak. A continuous 200 V/cm electric field applied between two plates bounding the ionization region accelerated the created ions into the 1 m long drift tube where the ions were detected by a multichannel electron multiplier. One hundred single particle mass spectra were averaged for each measurement. An example spectrum is included in Supporting Information.

2.3.2. Off-Line Measurement by SEM and AFM. Two off-line techniques were employed to understand the morphology of adsorbed oleic acid better. First, particles were collected on carbon tape attached to a stainless steel stub and imaged using a Hitachi S-4700 SEM with a field emission source. Collected particles were sputter-coated with 2 nm of an Au/Pd alloy (60/40) prior to analysis to enhance conductivity and improve image quality. Postprocessing of SEM images was performed using ImageJ.[32] Second, particles were also imaged using a multimode atomic force microscope (AFM) from Veeco Metrology group equipped with a Nanoscope IIIA control station in tapping-mode. The AFM was operated with silicon cantilevers having spring constants of 5.0 N/m at resonance frequencies of about 200 kHz (MikroMasch). Topographical and phase images were created by scanning the tip over a portion of the core particle surface.

3. Results

3.1. Characterization of Oleic Acid on Core Particles. ***3.1.1. ATOFMS and Velocimetry Analysis.*** In order to characterize the amount of oleic acid adsorbed onto the core particles, the mass spectrometry signal intensity for oleic acid was correlated to sample volume using pure oleic acid particles of known size. Oleic acid particles were either size-selected with a scanning mobility particle sizer (TSI Inc., model 3080) or introduced into the ATOFMS as a polydisperse aerosol with the mass spectral response sorted by particle size. Laser powers and temporal separation between IR and VUV firing were tuned to maximize the intensity of the M+ peak. The signal intensity of the M+ peak and the total integrated signal intensity at all masses scale linearly with laser fluence before reaching an asymptotic limit. It was previously argued[33] that this upper limit in total signal intensity is evidence for complete particle volatilization. The mechanism of particle evaporation is highly sensitive to the amount of energy imparted by the CO_2 laser. At laser fluences typical for the present work, evaporation of liquid organic droplets of similar size has been shown to proceed by thermal desorption whereby the molecules evaporate layer-by-layer.[34] Under these conditions, the measured signal intensity of pure oleic acid aerosol varied linearly with particle volume over the range from $0.3-25\ \mu m^3$.

As was done in the analysis of pure oleic acid particles, the M+ peak intensity for oleic acid adsorbed on the core particles was maximized by adjusting the CO_2 laser fluence. Aerosol core composition strongly influenced the optimal CO_2 laser energy for particle volatilization: 22.9 ± 1.4 mJ/pulse for both sizes of PSL spheres, 10.5 ± 2.0 mJ/pulse for 1.6 μm silica particles, and 4.7 ± 0.4 mJ/pulse for 3 μm porous silica particles. The difference in laser fluences by core type and the size dependence for the silica particles is attributed to enhanced absorption of the CO_2 laser radiation by the amorphous silica particle, which can transfer energy to the oleic acid on the particle surface. The M+ signal intensity on both core types is positively correlated with the oven vapor pressure of oleic acid present in the coating oven, as can be seen in Figure 2. Between three and seven measurements were performed at each vapor pressure, and each data point and error bar represents the mean and standard deviation ($\pm 1\sigma$) of the measurements. There is no

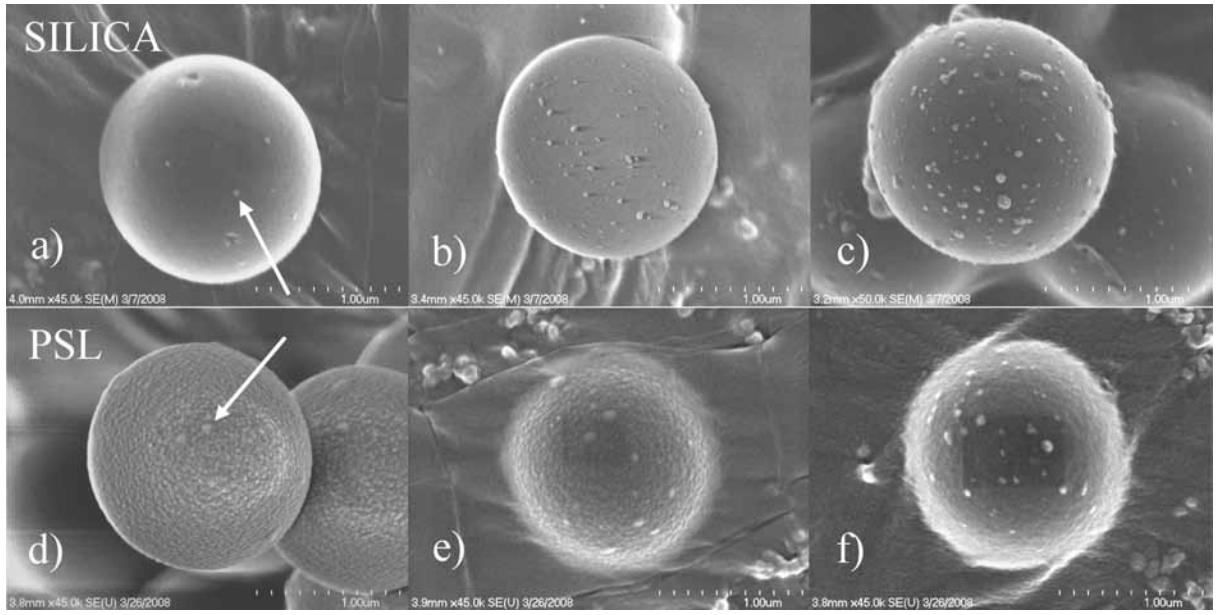

Figure 3. SEM images of core particles before and after exposure to oleic acid vapor. Surface features highlighted by the white arrows that are visible on (a) 1.6 μm silica and (d) 1.6 μm PSL particles before exposure to oleic acid may be adsorbed water. Oleic acid vapor adsorbs to core in islands that increase in number on both (b,c) silica and (e,f) PSL upon exposure to oleic acid vapor pressures of 1.2 and 4.3×10^{-3} Pa, respectively.

apparent enhancement in the M+ signal intensity due to capillary condensation on the porous silica particles, and the difference in signal intensity apparent for the two different core diameters of both core types scales roughly with the solid particle surface area. Under optimized desorption conditions, the M+ signal and the total ion signal (see Supporting Information) are similar for the two core types of each diameter, indicating that the amount of oleic acid accommodated by the inorganic cores prior to reaction is comparable. Based on the calibration of pure oleic acid, the signal intensity of oleic acid on each core particle was correlated to an adsorbed volume. These values suggested multilayer coverage for all core types, with coating thicknesses increasing from 5 to 30 nm over $P_{vap} = 1-6.5 \times 10^{-3}$ Pa assuming uniform distribution over the surface.

Velocimetry measurements of the vacuum aerodynamic diameter (d_{va}) by light-scattering in the ATOFMS and measurements of the aerodynamic diameter (d_a) by the APS did not indicate a detectable difference in size between the uncoated and the coated particles as would be expected from the ATOFMS coverage estimates. The ATOFMS and APS are capable of detecting a change in particle diameter of 6 and 16 nm, respectively, which is less than the 10−60 nm increase suggested by the ATOFMS calibration. As will be discussed below, there is both kinetic and imaging evidence that the morphology of the adsorbed oleic acid is not uniform, which changes the shape factor, χ, of the particle. Both d_{va} and d_a are inversely related to χ, which is defined as the ratio of resistance drag of the particle to that of a sphere having the same volume.[35] Adsorption of oleic acid increases χ and results in a decrease in the observed value for d_a and d_{va} relative to a uniform coating. Experimental determination of the particle density (ρ_p) and χ requires simultaneous measurement of d_{va} and the mobility diameter (d_m)[36,37] and as such is not possible for this system since supermicron particles can not be accurately sized by commercial mobility particle sizers. However, on the basis of values for χ measured for PSLs with varying coated morphologies,[38] the amount of oleic acid predicted to be adsorbed to the core particles based on the volume calibration should be observable within the sensitivity of velocimetry measurements by the ATOFMS and APS.

3.1.2. SEM Analysis. To reconcile the discrepancy between mass spectral and velocimetry measurements, particle microscopy was used to image the particles. Figure 3 shows images of 1.6 μm silica and 1.6 μm PSL particles before coating and after exposure to oleic acid vapor pressures of $P_{vap} = 1.2$ and 4.3×10^{-3} Pa. Some very small surface features are visible on core particles that do not pass through the coating oven (Figure 3a,d). Mass analysis of uncoated particles showed no signature of oleic acid or solvent preventing identification of the composition of these features. While the surface features on the uncoated core particles could merely be surface blemishes, it is hypothesized on the basis of kinetic information to be discussed below that these features are more likely to be residually adsorbed water, which was used along with methanol to suspend the core particles. With an ionization energy of 12.62 eV, water is not ionized by the 10.48 eV vacuum UV light and thus not detectable by the ATOFMS. Oleic acid adsorbed onto the core particles passing through the coating oven (Figure 3b,c,e,f) forms distinct regions, or islands, which are clearly observable and have also been shown to form during vapor-deposition of oleic acid onto flat silica and polystyrene surfaces in the absence of solvent.[39] Table 1 summarizes the average island geometry and coating characteristics based on analysis of collected SEM images using ImageJ. The oleic acid islands on both core types are 30−35 nm in height on average, which indicates a localized multilayer of oleic acid molecules. Interaction between the adsorbed oleic acid and the surface is expected to influence the orientation of molecules within an island. On silica, the carboxylic acid headgroup of oleic acid can participate in hydrogen bonding with surface silanol groups.[40,41] The similarity between island geometries on the two core types suggests that, even if the coordination of oleic acid to the PSL surface is different from the coordination to the silica surface, its orientation and packing may be similar. The orientation of oleic acid adsorbed to flat silica and polystyrene substrates has been shown to be nearly vertical with respect to the surface for islands that are a single molecule tall,[39] and multilayer adsorption may be

TABLE 1: Summary of Image Processing

substrate	oleic acid P_{vap} ($Pa \times 10^{-3}$)	height (nm)	width (nm)	SA/V (μm^{-1})	island coverage	oleic acid equiv. monolayers
PSL	no coating	20 ± 5	54 ± 13	99 ± 20	$1.2 \pm 0.4\%$	
	1.2	35 ± 10	75 ± 27	69 ± 30	$2.3 \pm 1.0\%$	0.20 ± 0.15
	4.3	34 ± 13	60 ± 24	85 ± 53	$3.4 \pm 0.8\%$	0.26 ± 0.2
silica	no coating	10 ± 3	23 ± 7	230 ± 83	$1.1 \pm 0.6\%$	
	1.2	30 ± 15	45 ± 18	123 ± 86	$2.5 \pm 1.1\%$	0.14 ± 0.13
	4.3	33 ± 8	44 ± 20	111 ± 63	$4.3 \pm 1.8\%$	0.32 ± 0.23

similar or some hybrid between this orientation and bulk "quasi-smectic" packing.[42] A stable, thermodynamically favorable geometry for the islands appears to be reached since the geometry of the average island does not change upon increasing the oleic acid P_{vap} from 1.2 to 4.3×10^{-3} Pa. Instead, the total number of islands increases with increasing oleic acid vapor pressure. It is possible that the condensation oven contained nanodroplets of oleic acid that deposited more efficiently onto the particles than the monomer oleic acid. APS measurements of the aerosol size distribution indicated the presence of submicrometer solvent or impurity particles that could not be removed during the aerosol conditioning process. Although these particles presented a significantly smaller surface area for condensation than core silica and PSL particles, they may still have served as seed particles for heterogeneous nucleation. The observation of islands cannot be entirely attributable to this process, however, because no such seed particles were measured during vapor deposition of oleic acid on the flat substrates.[39] On the basis of the average geometry of an adsorbed island and the proportion of the total core surface area that the islands covered, an estimate for the total volume of oleic acid on each particle surface was determined, correcting for adsorbed water. The effective surface layer thickness reported in Table 1 represents the ratio of the estimated volume of adsorbed oleic acid to the volume of oleic acid comprising a uniform monolayer coverage of the surface as determined from the molecular cross section, σ, of an oleic acid molecule in a monolayer (4.8×10^{-15} cm^2).[43] Effective surface layer thicknesses for both core types remain submonolayer over the range of oven conditions examined in this study.

3.1.3. AFM Analysis. The surface of uncoated and coated 1.6 μm particles was also characterized by AFM. The curvature of the aerosol particles made quantitative measurement of surface island height difficult, but phase imaging was able to differentiate the interaction of the AFM cantilever tip between the surface islands and the core particle. Phase measurements made on the surface of each core particle coated at $P_{vap} = 4.3 \times 10^{-3}$ Pa are shown in Figure 4. The bright regions apparent on the surface of both core types correspond to the oleic acid islands and are of similar size to those observed by SEM. Some distortion of the islands due to motion of the tapping tip is evident, but there remains a clear distinction between the interaction phase of the island and the core surface. Supporting our SEM island geometry estimates, this distinction suggests that the islands are adsorbed directly to the core particle surface rather than above a mono/multilayer of oleic acid. Recent examination of oleic acid sorption onto flat polystyrene and silica substrates shows that the contact angle for water on these surfaces decreases with deposition, indicating that the area not associated with the islands is likely to be devoid of any oleic acid.[39]

Except for the ATOFMS results, all methods to characterize particle morphology indicate that the total amount of oleic acid adsorbed to the core particles is less than a monolayer. An explanation for this discrepancy may be associated with the calibration of the ion mass spectrometry signal. Applying a signal-to-volume calibration for pure oleic acid to the coated particles may result in an overestimation of adsorbed mass due to a difference in the extent of evaporation by the CO_2 laser. The net surface area to volume ratio of the adsorbed oleic acid is much greater than that of a comparably sized pure oleic acid droplet. Under layer-by-layer thermal desorption, enhancement in the surface area to volume ratio may lead to greater evaporation efficiency. Additionally, matrix effects of the core particle are also likely to be contributing. The difference in optimized laser fluences for analysis demonstrates the fact that the core particle can absorb IR from the CO_2 laser and transfer energy to the adsorbed oleic acid.

3.2. Ozonolysis Kinetics of Adsorbed Oleic Acid. ***3.2.1. Dependence on Core Type and Coating Coverage.*** Previous kinetic analyses of pure oleic acid ozonolysis indicate that the reaction takes place predominately at or near the surface of the particle and is not limited by O_3 diffusion.[10,11,44,45] By investigating an adsorbed layer on a solid core with island thickness on the order of the estimated reacto-diffusive length of O_3 in oleic acid (10−20 nm), all of the oleic acid in these islands can be considered to be "on the surface". The surface concentration of oleic acid, $[Oleic]_{surf}$, can thus be defined as the average number concentration per unit surface area of the particle (molecules cm^{-2}). Similarly, the surface concentration of ozone, $[O_3]_{surf}$, can be defined as the number of dissolved ozone molecules per unit area of the particle, which is related via the Henry's law constant to the pressure of ozone in the flow tube. The rate of loss of oleic acid can then be expressed as

$$\frac{d[Oleic]_{surf}}{dt} = -k_2^{surf}[O_3]_{surf}[Oleic]_{surf} \quad (1)$$

The reaction rate of adsorbed oleic acid with ozone was calculated by monitoring the change in the M+ signal as a function of ozone exposure, which is the product of the ozone concentration in the flow tube and the time of interaction between the ozone and the aerosol. A series of experiments

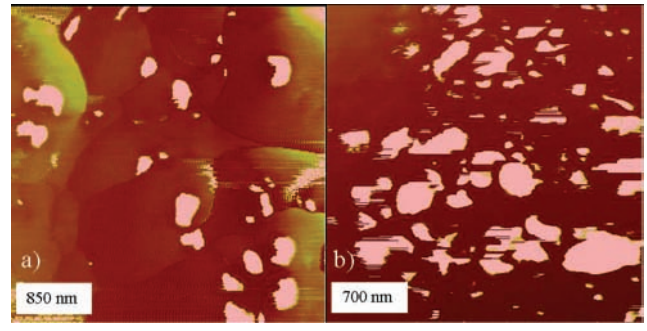

Figure 4. AFM phase images of (a) 1.6 μm silica and (b) 1.6 μm PSL particles exposed to an oleic acid vapor pressure of 4.3×10^{-3} Pa. Bright regions correspond to multilayer islands of adsorbed oleic acid. The length of the window mapped by the AFM tip for each image is noted in the inset.

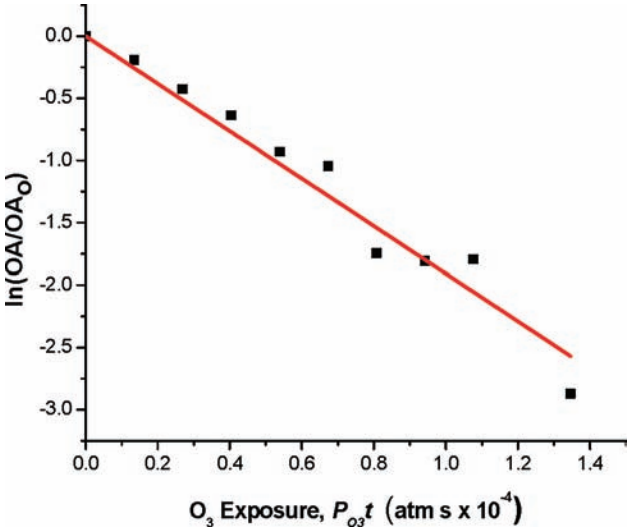

Figure 5. Typical decay of the relative adsorbed oleic acid signal upon exposure to O_3. The solid line represents a linear regression to the data from which the rate constant k_1' is determined.

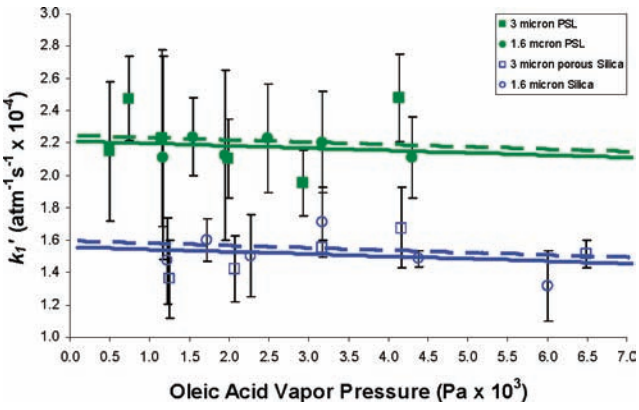

Figure 6. Summary of observed rate constants for ozonolysis of adsorbed oleic acid as a function of oleic acid vapor pressure in the coating oven. Solid (1.6 μm diameter core particles) and dashed (3 μm diameter core particles) lines represent the results of a random-effects meta regression analysis. The difference in the rate constants between the two core types is statistically significant ($p < 0.001$). No association was found between the particle size or oleic acid vapor pressure and the rate constants ($p \geq 0.5$ for each).

investigating the effect of surface coverage on the observed kinetics was performed on PSL and silica particles of both sizes. O_3 in the flow tube was held at $2.1 \pm 0.3 \times 10^{14}$ molecules cm^{-3} (8.4 ppm), in excess of oleic acid by at least a factor of 35, such that the ozonolysis reaction can be considered pseudo-first-order. This condition is demonstrated by the results of a typical loss of relative oleic acid signal upon exposure to O_3 ($P_{O_3}\,t$) as shown in Figure 5. A linear regression describes the data well and yields a pseudo-first-order rate constant, k_1' (atm^{-1} s^{-1}), for the reaction of oleic acid and ozone on each inorganic core. Figure 6 shows a summary of pseudo-first-order rate constants measured for oleic acid ozonolysis on PSLs and silica aerosol particles and the results of a random-effects meta-regression (see Supporting Information for details). Between three and seven experiments were performed at each oleic acid vapor pressure, and each data point and error bar represents the mean and standard deviation ($\pm 1\sigma$) of the measurements. The average values for k_1' on PSLs are $2.17 \pm 0.06 \times 10^4$ atm^{-1} s^{-1} and $2.25 \pm 0.20 \times 10^4$ atm^{-1} s^{-1} for 1.6 and 3 μm diameter particles, respectively. The average values for k_1' on silica are $1.51 \pm 0.13 \times 10^4$ atm^{-1} s^{-1} and $1.52 \pm 0.12 \times 10^4$ atm^{-1} s^{-1} for nonporous 1.6 μm and porous 3 μm diameter particles, respectively. The key findings of the experiments are that (1) oleic acid vapor pressure did not have a statistically significant association with kinetic rate, (2) core particle size did not have a statistically significant association with kinetic rate, and (3) at a given particle size and oleic acid vapor pressure, the kinetic rate for reaction on PSL particles was $0.65 \pm 0.18 \times 10^4$ atm^{-1} s^{-1}, or 43% faster than that for silica particles.

3.2.2. Dependence of the Observed Rate Constant on O_3 Concentration. Surface reactions involving oxidation of submonolayer organic coatings by O_3 have frequently been shown to proceed through a surface-mediated Langmuir−Hinshelwood (LH) mechanism rather than a direct bimolecular Eley−Rideal mechanism.[24−28] Under a surface-mediated reaction, O_3 becomes bound to available surface sites prior to reaction and the observed first-order kinetics exhibit a distinctly nonlinear relationship with increasing [O_3] as the surface becomes saturated. The formulation of the LH mechanism applied to reaction of O_3 with submonolayer benzo-a-pyrene by Poschl et al.[24] and formalized more generally by Ammann et al.[46] has been adopted widely in subsequent work. Under this formulation, oxidant molecules are assumed to adsorb with equal probability both to the exposed core surface and to the surface-bound organic molecules, and the resulting LH expression for the apparent first-order rate constant, k_1 (s^{-1}), is

$$k_1 = \frac{k_{1,\max} K_{O_3}[O_3]}{1 + K_{O_3}[O_3]} \qquad (2)$$

where $k_{1,max}$ is the product of the second order rate constant, k_2, and the number of available surface sites for adsorption [SS], and K_{O_3} is the equilibrium partition constant for O_3 between gas and condensed phases. The composition of the substrate to which an organic surfactant is adsorbed has been shown to influence the observed Langmuir−Hinshelwood kinetics between O_3 and surfactant layer.[26,27] There is a dearth of literature on the application of the LH mechanism to adsorbate−adsorbate interactions involving the presence of surface islands. What research has been done has focused exclusively on the catalyst-enhanced reaction between O and CO.[47,48] We apply the LH model here by treating each surface island as a "composite reactant molecule". The limitations of this approach will be discussed in section 4.

Flow tube experiments on both 1.6 μm PSL and 1.6 μm silica particles were performed over a range of O_3 concentrations for a coating $P_{vap} = 4.3 \times 10^{-3}$ Pa to evaluate whether O_3 interaction with the bare core particle surface participates in the oxidation mechanism of adsorbed oleic acid. The apparent first-order rate constant was evaluated directly from the relationship between the relative oleic acid signal loss and the reaction time rather than ozone exposure in order to determine an explicit [O_3] dependence. A summary of experimental values for k_1 is shown in Figure 7. The trend for oleic acid ozonolysis on PSL particles is clearly nonlinear, indicating that the particle surface is reaching saturation with O_3. The weighted nonlinear least-squares fit of eq 2 to the PSL data is shown in Figure 7 along with the $\pm 1\sigma$ confidence intervals. The LH parameters derived from this fit are $k_{1,max} = 0.64 \pm 0.10$ s^{-1} and $K_{O_3} = 2.14(\pm 0.57) \times 10^{-15}$ cm^3 molecule^{-1}. The observed rate constant for the reaction on silica particles is systematically lower than the corresponding value on PSL particles below [O_3] $= 5 \times 10^{14}$ molecules cm^{-3} but appears to become faster than the reaction on PSL particles at the highest [O_3] explored. Although the first order kinetics on silica do not exhibit obvious curvature over the range of [O_3] investigated in this study, a nonlinear least-

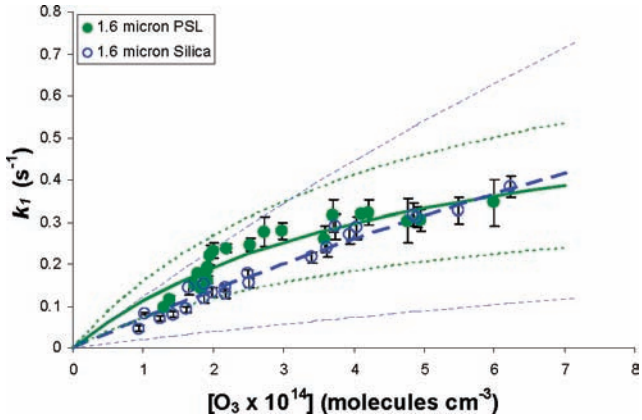

Figure 7. [O_3] dependence of the pseudo-first-order rate constant for ozonolysis of adsorbed oleic acid on 1.6 μm core particles of PSL and silica. Oleic acid $P_{vap} = 4.3 \times 10^{-3}$ Pa. A Langmuir−Hinshelwood curve (solid line) for the PSL data and for the (long-dashed line) silica data are also included along with the corresponding 1σ confidence intervals for each fit (short-dashed lines).

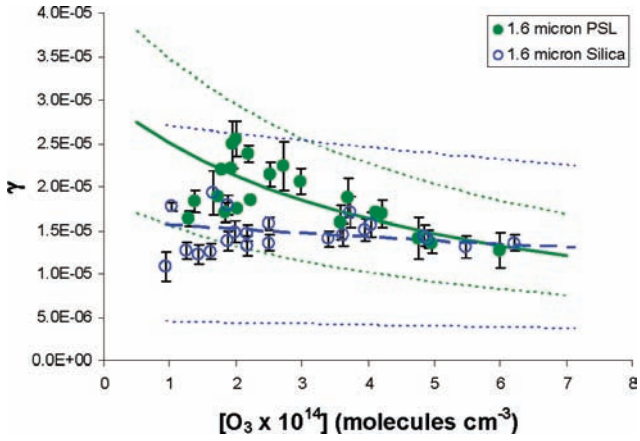

Figure 8. [O_3] dependence of the uptake coefficient, γ, for ozonolysis of adsorbed oleic acid on 1.6 μm core particles of PSL and silica. Oleic acid $P_{vap} = 4.3 \times 10^{-3}$ Pa. 1σ confidence intervals for each fit (short-dashed lines) are reported.

squares fit of eq 2 to the silica data can still be performed under the assumption that saturation will occur at higher [O_3]. The resulting LH parameters derived from the fit of eq 2 to the silica data are $k_{1,max} = 2.2 \pm 1.1$ s^{-1} and $K_{O_3} = 3.59(\pm 2.13) \times 10^{-16}$ cm^3 $molecule^{-1}$. Differences in the PSL and silica fit parameters will be discussed below.

3.2.3. Determination of Uptake Coefficients. Because values for rate constants are influenced by experimental conditions, interstudy comparisons are facilitated by expressing results of aerosol kinetic studies in terms of a reaction probability, or uptake coefficient, γ. The parameter γ represents the ratio of the number of collisions between two reactants that result in a chemical transformation to the total number of collisions that occur. When considering heterogeneous reactions between a gas phase oxidant and a surface bound organic, the magnitude of γ is influenced by the choice of which reactant to use as a frame of reference. For example, the reaction probability for oxidation of liquid aerosols such as pure oleic acid or multicomponent mixtures of oleic acid is typically taken from the perspective of O_3 whereby γ represents the net rate of loss of the gas-phase species normalized to the gas-particle collision rate. Under the assumption that interaction between O_3 and oleic acid provides the sole loss mechanism for both species, the reaction probability from the perspective of O_3 is expressed as

$$\gamma_{O_3} = \frac{4k_1 n_{oleic}}{\bar{c}_{O_3}[O_3]SA} \quad (3)$$

where n_{oleic} is the total number of oleic acid molecules available for reaction, $\bar{c}_{O_3}$ is the mean kinetic speed of O_3, and SA is the surface area of the particle. Typical values for γ_{O_3} for pure oleic acid are approximately 10^{-3}, representing one reaction per thousand collisions.[8,11,45] However, applying this formulation to the case where the surfactant layer does not uniformly cover the substrate presents some challenges in defining the reactive surface area. As a result, analysis of kinetics of surface and, more specifically, submonolayer reactions, have typically made use of a different parametrization of the uptake coefficient with the surfactant as a frame of reference. We follow this convention here and define γ as the number of oleic acid molecules at the surface lost relative to the ozone-surface organic collision frequency, which can be expressed as[46]

$$\gamma_{oleic} = \frac{4k_1}{\bar{c}_{O_3}\sigma_{oleic}[O_3]} \quad (4)$$

where σ_{oleic} is the molecular cross section of oleic acid. Since the reaction between O_3 and oleic acid has been monitored by observation of the loss of oleic acid rather than the loss of O_3, the latter formulation appears to be more appropriate for the current system. Employing γ_{oleic} assumes that each oleic acid molecule on the surface is equally accessible to reaction by O_3, but given that the geometry of the island is similar to the reacto-diffusive length for O_3 in oleic acid, this seems reasonable. A discussion of how the resulting values for γ_{oleic} may differ from γ_{O_3} is addressed below. Figure 8 shows the calculated values for γ_{oleic} based on the experimental data from Figure 7 as well as the approximation to the PSL (solid line) and silica (dashed line) data based on the LH fitting parameters. Values for γ_{oleic} for reaction of oleic acid on PSLs decrease from 2.7×10^{-5} to 1.2×10^{-5} with increasing [O_3], overlapping at high [O_3] with the estimated value of γ_{oleic} for silica, which decreases from 1.6×10^{-5} to 1.3×10^{-5}. At lower O_3 concentrations, γ_{oleic} is higher on PSL than silica, suggesting that the estimated lifetime of oleic acid adsorbed to different inorganic particle types in the atmosphere may depend both on the nature of the inorganic substrate and on the local O_3 concentration.

4. Discussion

4.1. Influence of Island Morphology on Kinetics. While previous laboratory studies have reported ozonolysis kinetics of submonolayer surfactants,[24,27,28] this study is the first to our knowledge to observe the ozonolysis kinetics of multilayer surfactant islands on coated aerosol particles. Such a morphology may have atmospheric relevance since microscopy and spectromicroscopy of ambient particles have shown that organic coatings are often internally mixed with inorganic particles such as dust and that the fraction of the total particle surface covered by organic material is highly variable.[22,23]

As a surface reaction, the observed oxidation kinetics between O_3 and adsorbed oleic acid are expected to sensitively depend on the morphology of the multilayer islands and on how the islands grow with increasing oleic acid deposition because this dictates the interfacial surface area. The observed constant kinetics with increasing oleic acid surface coverage can thus be explained by the fact that the islands of oleic acid formed during vapor deposition onto 1.6 μm PSL and 1.6 μm silica core particles do not appear to change in size as the total coverage of oleic acid on the core particle surface increases,

resulting in an invariance of the surface to volume ratio of oleic acid encountered by O_3. In this sense, the multilayer islands of oleic acid react similarly with O_3 to submonolayer coatings of organic surfactant layers. Previous submonolayer studies also noted invariant pseudo-first-order kinetics of O_3 uptake by benzo-a-pyrene on submicrometer aerosols[24,26] or by oleic acid on suspended water droplets.[49] However, surfactant coatings above one monolayer, where the coating occurs evenly on the surface so that the underlying substrate is not exposed, have exhibited a significant decrease in the observed rate constants.[24,26,50] A recent study by Katrib et al. also investigated the ozonolysis of oleic acid adsorbed to PSL particles, though much smaller (100 nm) than that used in this study, and were able to measure oleic acid coating thicknesses between 2−30 nm by measurement of the aerosol mobility diameter.[29] These coatings would represent multilayer adsorption of oleic acid to the PSL core assuming a uniform coating and, although kinetic information was not published, it was confirmed through private correspondence that no difference in the ozonolysis kinetics was observed between the oleic acid coating thicknesses investigated by Katrib et al.[51] This suggests that oleic acid islands were also likely to have been formed in the Katrib et al. study.

Adaptation of a Langmuir−Hinshelwood reaction model to incorporate the presence of two-dimensional surface islands for one of the adsorbates showed that the primary difference in the behavior of the new model to a simple LH mechanism was due to the definition of surface sites occupied by the island-forming adsorbate and the resulting lateral interactions between the other adsorbate molecules on the remaining surface sites.[48] Since eq 2, which has successfully described the interaction of O_3 and submonolayer coverage of organics, does not distinguish between the ability of O_3 to adsorb directly to the core or its ability to adsorb onto oleic acid, there is no distinction between these systems in two dimensions. The geometry of the average surface islands leaves approximately 10% of an individual island at a penetration depth greater than the calculated reacto-diffusive length of O_3 in oleic acid, such that the appropriateness of applying eq 2 to a three-dimensional island must be addressed. It is possible that this small fraction of oleic acid in the center of the island is somehow limited in its ability to self-diffuse to the oleic acid/air interface and requires a transition between a surface-dominated reaction and one determined by O_3 diffusion in the island. However, the excellent agreement of a single component exponential fit for all OA decays indicates that this cannot be the case within the sensitivity of the current measurements. Additionally, the agreement of the exponential fit with the data also suggests that there is no appreciable lateral interaction between adsorbed O_3 molecules as a result of the island formation, which has been shown to perturb initial slopes of decay.[47] As a result, the application of eq 2 to describe the interaction of oleic acid and O_3 for the current system is believed to be appropriate.

4.2. Influence of Core Particle Size and Porosity on Kinetics. Although the geometry of oleic acid islands on 3 μm solid PSL and porous silica core particles was not measured by SEM and AFM analysis, the fact that the ozonolysis reaction rate is not statistically different than the rate measured on the respective 1.6 μm core particles indicates that the arrangement of oleic acid on the surface of the larger particles must be similar to their smaller counterparts. There is also no evidence for hindrance of the reaction by pore confinement. This finding is perhaps the most surprising aspect of this study. The prior expectation was that oleic acid trapped inside the porous particle would have reacted more slowly because of diffusion of O_3 into the pores or physical constraints on oleic acid due to confinement in the pores. However, the surface analysis suggests either that the oleic acid never penetrated inside the porous silica particle so that the porosity had no effect on the kinetics or that oleic acid trapped in the pores was not efficiently desorbed by the CO_2 laser. Thus, the question of how efficiently ozone attacks trapped oleic acid inside particles remains an open question.

4.3. Influence of Core Particle Type on Kinetics. Interpretation of the fit parameters derived from applying eq 2 to the observed O_3 dependence on the rate constant suggests that two separate phenomena are responsible for the difference in the ozonolysis rate due to the nature of the core illustrated in Figures 6 and 7. The higher reactivity of oleic acid on the PSL spheres is likely to be the result of more efficient partitioning of O_3 to the PSL surface than to that of the silica surface, and the faster reaction on the silica particles at high O_3 concentrations may be due to differences in the ability of O_3 to attack the oleic acid double bond associated with the orientation or packing of oleic acid on the two surfaces. Both phenomena can be addressed in terms of the LH parameters K_{O_3} and $k_{1,max}$ derived for reaction on PSL and silica and will now be discussed at greater length.

The equilibrium constant defining the partitioning of O_3 between the surface adsorption onto the core particle and the gas phase, K_{O_3}, is a factor of 6 times greater for the PSL surface than for the silica surface indicating that O_3 is bound more strongly to the less polar PSL surface. This preference is consistent with the trend in K_{O_3} values for substrates of different polarities summarized by Kwamena et al.[27] and indicates that an O_3 molecule has a longer residence time on the surface of the PSL particles. With a longer residence time comes more opportunities to encounter an oleic acid double bond, which explains why the reaction between oleic acid and O_3 is faster on the PSL surface.

While the trend in K_{O_3} values for PSL and silica measured in this study is consistent with previous measurements for K_{O_3}, the magnitude of the values are not in obvious agreement. Although pure polystyrene is nonpolar, the value for K_{O_3} on PSL core particles is significantly smaller than that measured for strongly nonpolar surfaces such as soot[24] and more closely resembles the K_{O_3} of the oxygenated surface of azelaic acid.[27] We believe this is partly a result of the presence of water coadsorbed to the PSL surface. The K_{O_3} value for silica is much lower than most K_{O_3} values reported, even below the value for partitioning to the surface of water (4.66×10^{-16} cm^3 molecule^{-1}),[25] and indicates that O_3 is bound very loosely if at all to the surface of the silica particles. A linear dependence between k_1 and O_3, indicative of an Eley−Rideal mechanism, has been measured previously for ozone oxidation of a surface-active organic, benzo-a-pyrene, sorbed to silica [50,52] and may be due in part to reaction between ozone and exposed silica surfaces,[53] which can be competitive with chemical reaction on surfaces with submonolayer surfactant coverage.[54]

The larger value of $k_{1,max}$ for the reaction on the silica particles indicates that, although O_3 likely has a longer residence time on the PSL surface, the reaction between oleic acid and O_3 is ultimately more efficient on the silica surface. This implies that, although the measured island geometries for oleic acid on the two core types are similar, the core composition may also alter the orientation or packing of the oleic acid on the two surfaces. Numerical simulations suggest that the orientation of long chain unsaturated molecules affects their reactivity with ozone,[55] and the different polarities between the hydrophilic silica and the hydrophobic polystyrene may result in different strengths and

geometries of the oleic acid/substrate interaction on the two surfaces. The "quasi-smectic" self-coordination between oleic acid molecules observed in bulk solutions[42] has been hypothesized to influence its reactivity with ozone,[45] and anything that disrupts this interaction could change the accessibility of the double bond to attack by O_3.

The orientation of the oleic acid in the multilayer islands on both surfaces may be different than for a uniform submonolayer coating of oleic acid. A recent study by McNeill et al., for the ozonolysis of aqueous salt particles covered with ~0.9 monolayers of sodium oleate, measured a $k_{1,max}$ of 0.05 s^{-1}, over an order of magnitude different from the values in this study.[28] However, the resulting $\gamma_{oleic} \approx 10^{-5}$ reported by McNeill et al. is in good agreement with the results reported in Figure 8. Both of these results stand in contrast to the probability of reaction between O_3 and oleic acid on a suspended water droplet, $\gamma_{O_3} = 2.6 \times 10^{-6}$, reported recently.[49] This discrepancy may be due to differences in packing of oleic acid in the different studies. Gonzalez-Labrada et al. injected oleic acid onto the surface of a suspended water droplet and then removed volume from the water droplet to create a monolayer of oleic acid at the surface of the drop.[49] Compressing the insoluble monolayer of oleic acid is likely to alter its packing geometry as well as the molecular cross section of an oleic acid molecule.

The presence of adsorbed islands creates inherent difficulties in direct comparisons between literature values for the uptake coefficient calculated from the perspective of an O_3 molecule (eq 3) and values for the uptake coefficient calculated from the perspective of an oleic acid molecule (eq 4). In order to calculate γ_{O_3} for the present morphology, a decision about how to define the reactive surface area of the particle is required, which can be ambiguous. If, for example, O_3 was assumed to react exclusively with oleic acid and the surface area of the islands alone was used to define SA, the resulting values for γ_{O_3} for the reaction on silica would range from 1.2×10^{-4} to 9.8×10^{-5} over the range of $[O_3]$ investigated, which is over an order of magnitude higher than the values of γ_{oleic}. Yet, how the reactive surface area is defined should probably depend on the partitioning coefficient, K_{O_3}, which determines how long the ozone stays on the surface before desorbing. By scaling the number of collisions O_3 makes with the uncoated surface of the core particle by the factor $K_{O_3}[O_3]$ to account for desorption, the resulting values for γ_{O_3} would range from 7.1×10^{-5} to 1.9×10^{-5} over the range of $[O_3]$ investigated. Finally, if the total surface area of the particle was used to define SA_{oleic}, the resulting value for γ_{O_3} would be 5.3×10^{-6}, which is similar to the value reported by Gonzalez-Labrada et al.[49] It becomes clear that, although the uptake coefficient was intended to be a parameter that can be compared directly across experiments, one must pay close attention to how γ has been parametrized. Under all scenarios, however, the resulting uptake coefficient for the reaction involving adsorbed oleic acid is lower than literature values reported for pure oleic acid, indicating that the matrix effects associated with the coated particle morphology are slowing the reaction.

5. Conclusions and Atmospheric Implications

The rate of the surface reaction between surface-adsorbed oleic acid and O_3 has been shown for the first time to be influenced by the composition of the aerosol substrate. The reaction is ultimately more efficient on the silica surface but proceeds faster on the less polar PSL core at lower $[O_3]$ because of the increased residence time of O_3 on the PSL surface. Invariant geometry of the adsorbed islands on both core types resulted in no kinetic dependence on oleic acid coverage or core particle surface area. As with so many kinetic studies of aerosols, these observations could be the result of multiple variables that were not effectively isolated. As such, this study raises many questions that it cannot answer, such as how the orientation of adsorbed oleic acid orients changes on different substrates, how this orientation may change as these islands grow or coalesce into multilayers, and whether oleic acid trapped in a pore network reacts differently than oleic acid adsorbed to a surface. Nevertheless, these results indicate that the estimated lifetime of surface-adsorbed oleic acid, and likely similar unsaturated organics, by O_3 in the atmosphere will be affected by core composition and will be longer than the lifetime of a comparable amount of pure oleic acid. The different chemical aging experienced by adsorbed oleic acid is another example of the important role that particle morphology has in controlling aerosol reactivity and may help to explain the current discrepancy between laboratory and field measurements.[56]

Acknowledgment. This work is funded by a grant from the NSF (NSF Award No. 0509837). We thank Joel Thornton and Scot Martin for useful discussions, the Sheiko group for help with and use of their AFM equipment, and finally Kimberly Powers for assistance in development of the meta-regression analysis.

Supporting Information Available: Comparison of oleic acid fragmentation on the two core particles, comparison of total signal intensity with coverage, description of meta-regression analysis. This information is available free of charge via the Internet at http://pubs.acs.org.

References and Notes

(1) Lee, S.-H.; Murphy, D. M.; Thompson, D. S.; Middlebrook, A. M. Chemical components of single particles measured with Particle Analysis by Laser Mass Spectrometry (PALMS) during the Atlanta SuperSite Project: Focus on organic/sulfate, lead, soot, and mineral particles. *J. Geophys. Res.* **2002**, *107*, 1–1.

(2) Cabada, J. C.; Rees, S.; Takahama, S.; Khlystov, A.; Pandis, S. N.; Davidson, C. I.; Robinson, A. L. Mass size distributions and size resolved chemical composition of fine particulate matter at the Pittsburgh supersite. *Atmos. Environ.* **2004**, *38* (20), 3127–3141.

(3) Limbeck, A.; Puxbaum, H. Organic acids in continental background aerosols. *Atmos. Environ.* **1999**, *33* (12), 1847–1852.

(4) Hinz, K.-P.; Trimborn, A.; Weingartner, E.; Henning, S.; Baltensperger, U.; Spengler, B. Aerosol single particle composition at the Jungfraujoch. *J. Aerosol Sci.* **2005**, *36*, 123–145.

(5) Finlayson-Pitts, B. J.; Pitts, J. N. *Chemistry of the Upper and Lower Atmosphere: Theory, Experiments and Applications*; Academic Press: New York, 2000.

(6) Seinfeld, J. H.; Pandis, S. N. *Atmospheric Chemistry and Physics;* Wiley Interscience: New York, 1998.

(7) Zahardis, J.; Petrucci, G. A. The oleic acid-ozone heterogeneous reaction system: products, kinetics, secondary chemistry, and atmospheric implications of a model system - a review. *Atmos. Chem. Phys.* **2007**, *7*, 1237–1274.

(8) Moise, T.; Rudich, Y. Reactive Uptake of Ozone by Aerosol-Associated Unsaturated Fatty Acids: Kinetics, Mechanism, and Products. *J. Phys. Chem. A* **2002**, *106*, 6469–6476.

(9) Thornberry, T. D.; Abbatt, J. P. D. Heterogeneous reaction of ozone with liquid unsaturated fatty acids: detailed kinetics and gas-phase product studies. *Phys. Chem. Chem. Phys.* **2004**, *6*, 84–93.

(10) Smith, G. D.; Woods III, E.; Hauser, C.; Miller, R. E.; Baer, T. Reactive uptake of ozone by oleic acid aerosol particles: Application of single particle mass spectrometry to heterogeneous reaction kinetics. *J. Phys. Chem. A* **2002**, *106*, 8085–8095.

(11) Morris, J. W.; Davidovits, P.; Jayne, J. T.; Shi, Q.; Kolb, C. E.; Worsnop, D. R.; Barney, W. S.; Jimenez, J.; Cass, G. R. Kinetics of submicron oleic acid aerosols with ozone; a novel aerosol mass spectrometric technique. *Geophys. Res. Lett.* **2002**, *29*, 711−71/4.

(12) Rogge, W. F.; Hildemann, L. M.; Mazurek, M. A.; Cass, G. R.; Simoneit, B. R. T. Sources of fine organic aerosol 1. Charbroiler and meat cooking operations. *Environ. Sci. Technol.* **1991**, *25*, 1112–1119.

(13) Nash, D. G.; Tolocka, M. P.; Baer, T. The uptake of O_3 by myristic acid-oleic acid mixed particles: evidence for solid surface layers. *Phys. Chem. Chem. Phys.* **2006**, *8*, 4468–4475.

(14) Katrib, Y.; Biskos, G.; Buseck, P. R.; Davidovits, P.; Jayne, J. T.; Mochida, M.; Wise, M. E.; Worsnop, D. R.; Martin, S. T. Ozonolysis of Mixed Oleic-Acid/Stearic-Acid Particles: Reaction Kinetics and Chemical Morphology. *J. Phys. Chem. A* **2005**, *109* (48), 10910–10919.

(15) Knopf, D. A.; Anthony, L. M.; Bertram, A. K. Reactive Uptake of O3 by Multicomponent and Multiphase Mixtures Containing Oleic Acid. *J. Phys. Chem. A* **2006**, *109* (25), 5579–5589.

(16) Hearn, J. D.; Smith, G. D. Measuring Rates of Reaction in Supercooled Organic Particles with Implications for Atmospheric Aerosol. *Phys. Chem. Chem. Phys.* **2005**, *7* (13), 2549–2551.

(17) Hearn, J. D.; Smith, G. A. Ozonolysis of mixed oleic acid/n-docosane particles: The roles of phase, morphology, and metastable states. *J. Phys. Chem. A* **2007**, *111* (43), 11059–11065.

(18) Buseck, P. R.; Posfai, M. Airborne minerals and related aerosol particles: Effects on climate and the environment. *Proc. Natl. Acad. Sci. U. S. A.* **1999**, *96* (7), 3372–3379.

(19) Tervahattu, H.; Juhanoja, J.; Vaida, V.; Tuck, A. F.; Niemi, J. V.; Kupiainen, K.; Kulmala, M.; Vehkamaki, H. Fatty acids on continental sulfate aerosol particles. *J. Geophys. Res. Atmos.* **2005**, 110 D6.

(20) Tervahattu, H.; Juhanoja, J.; Kupiainen, K. Identification of an organic coating on marine aerosol particles by TOF-SIMS. *J. Geophys. Res. Atmos.* **2002**, 107 D16.

(21) Mochida, M.; Umemoto, N.; Kawamura, K.; Lim, H. J.; Turpin, B. J. Bimodal size distributions of various organic acids and fatty acids in the marine atmosphere: Influence of anthropogenic aerosols, Asian dusts, and sea spray off the coast of East Asia. *J. Geophys. Res. Atmos.* **2007**, 112 D15.

(22) Russell, L. M.; Maria, S. F.; Myneni, S. C. B. Mapping organic coatings on atmospheric particles. *Geophys. Res. Lett.* **2002**, *29*, 16.

(23) Falkovich, A. H.; Schkolnik, G.; Ganor, E.; Rudich, Y. Adsorption of organic compounds pertinent to urban environments onto mineral dust particles. *J. Geophys. Res. Atmos.* **2004**, 109 D2.

(24) Poschl, U.; Letzel, T.; Schauer, C.; Niessner, R. Interaction of ozone and water vapor with spark discharge soot aerosol particles coated with benzo[a]pyrene: O-3 and H2O adsorption, benzo[a]pyrene degradation, and atmospheric implications. *J. Phys. Chem. A* **2001**, *105* (16), 4029–4041.

(25) Mmereki, B. T.; Donaldson, D. J. Direct observation of the kinetics of an atmospherically important reaction at the air-aqueous interface. *J. Phys. Chem. A* **2003**, *107*, 11038–11042.

(26) Kwamena, N. O. A.; Thornton, J. A.; Abbatt, J. P. D. Kinetics of surface-bound benzo[a]pyrene and ozone on solid organic and salt aerosols. *J. Phys. Chem. A* **2004**, *108* (52), 11626–11634.

(27) Kwamena, N. O. A.; Staikova, M. G.; Donaldson, D. J.; George, I. J.; Abbatt, J. P. D. Role of the aerosol substrate in the heterogeneous ozonation reactions of surface-bound PAHs. *J. Phys. Chem. A* **2007**, *111* (43), 11050–11058.

(28) McNeill, V. F.; Wolfe, G. M.; Thornton, J. A. The Oxidation of Oleate in Submicron Aqueous Salt Aerosols: Evidence of a Surface Process. *J. Phys. Chem. A* **2007**, *111* (6), 1073–1083.

(29) Katrib, Y.; Martin, S. T.; Hung, H. M.; Rudich, Y.; Zhang, H.; Slowik, J. G.; Davidovits, P.; Jayne, J. T.; Worsnop, D. R. Products and Mechanisms of Ozone Reactions with Oleic Acid for Aerosol Particles Having Core-Shell Morphologies. *J. Phys. Chem. A* **2004**, *108*, 6686–6695.

(30) Tang, I. N.; Munkelwitz, H. R. Determination of Vapor Pressure from Droplet Evaporation Kinetics. *J. Colloid Interface Sci.* **1990**, *141* (1), 109–118.

(31) Sykes, C.; Woods III, E.; Smith, G. D.; Baer, T.; Miller, R. E. Thermal Vaporization−Vacuum Ultraviolet Laser Ionization Time of Flight Mass Spectrometry of Single Aerosol Particles. *Anal. Chem.* **2001**, *73*, 2048–2052.

(32) Abramoff, M. D.; Magelhaes, P. J.; Ram, S. J. Image Processing with Image. *J. Biophotonics International* **2004**, 36–42.

(33) Woods III, E.; Smith, G. D.; Dessiaterik, Y.; Baer, T.; Miller, R. E. Quantitative detection of aromatic compounds in single aerosol particle mass spectrometry. *Anal. Chem.* **2001**, *73*, 2317–2322.

(34) Woods III, E.; Smith, G. D.; Miller, R. E.; Baer, T. Depth-profiling of heterogeneously mixed aerosol particles using single particle mass spectrometry. *Anal. Chem.* **2002**, *74*, 1642–1649.

(35) Hinds, W. C. *Aerosol Technology: Properties, Behavior, and Measurement of Airborne Particles; 2nd ed.;* Wiley-Interscience: New York, 1999.

(36) Zelenyuk, A.; Cai, Y.; Imre, D. From Agglomerates of Spheres to Irregularly Shaped Particles: Determination of Dynamic Shape Factors from Measurements of Mobility and Vacuum Aerodynamic Diameters. *Aerosol Sci. Technol.* **2006**, *40*, 197–217.

(37) DeCarlo, P. F.; Slowik, J. G.; Worsnop, D. R.; Davidovits, P.; Jimenez, J. L. Particle Morphology and Density Characterization by Combined Mobility and Aerodynamic Diameter Measurements. Part 1: Theory. *Aerosol Sci. Technol.* **2004**, *38*, 1185–1205.

(38) Cai, Y.; Zelenyuk, A.; Imre, D. A high resolution study of the effect of morphology on the mass spectra of single PSL particles with Na-containing layers and nodules. *Aerosol Sci. Technol.* **2006**, *40* (12), 1111–1122.

(39) Garland, E. R.; Rosen, E. P.; Clarke, L. I.; Baer, T. Structure of submonolayer oleic acid coverages on inorganic aerosol particles: evidence of island formation. *Phys. Chem. Chem. Phys.* **2008**, *10* (21), 3156–3161.

(40) Blyholder, G.; Adhikar, C.; Proctor, A. Structure and Orientation of Oleic-Acid Adsorbed Onto Silica-Gel. *Colloids Surf. A-Physicochem. Eng. Aspects* **1995**, *105* (1), 151–158.

(41) Lee, D. H.; Condrate, R. A. FTIR spectral characterization of thin film coatings of oleic acid on glasses: I. Coatings on glasses from ethyl alcohol. *J. Mater. Sci.* **1999**, *34* (1), 139–146.

(42) Iwahashi, M.; Kasahara, Y.; Matsuzawa, H.; Yagi, K.; Nomura, K.; Terauchi, H.; Ozaki, Y.; Suzuki, M. Self-Diffusion, Dynamical Molecular Conformation, and Liquid Structures of n-Saturated and Unsaturated Fatty Acids. *J. Phys. Chem. B* **2000**, *104*, 6186–6194.

(43) Langmuir, I. The shapes of group molecules forming the surfaces of molecules. *Proc. Natl. Acad. Sci.* **1917**, *3*, 251–257.

(44) Moise, T.; Rudich, Y. Reactive uptake of ozone by proxies for organic aerosols: Surface versus bulk processes. *J. Geophys. Res.* **2000**, *105*, 14667–14676.

(45) Hearn, J. D.; Lovett, A. J.; Smith, G. D. Ozonolysis of Oleic Acid Particles: Evidence for a Surface Reaction and Secondary Reactions Involving Criegee Intermediates. *Phys. Chem. Chem. Phys.* **2005**, *7* (3), 501–511.

(46) Ammann, M.; Poschl, U.; Rudich, Y. Effects of reversible adsorption and Langmuir-Hinshelwood surface reactions on gas uptake by atmospheric particles. *Phys. Chem. Chem. Phys.* **2003**, *5* (2), 351–356.

(47) Hellsing, B.; Zhdanov, V. P. The Island Model of A Langmuir-Hinshelwood Reaction. *Chem. Phys. Lett.* **1988**, *147* (6), 613–618.

(48) Graham, W. R. C.; Lynch, D. T. Island Models and the Catalytic-Oxidation of Carbon-Monoxide. *Surf. Sci.* **1987**, *187* (1), L633−L638.

(49) Gonzalez-Labrada, E.; Schmidt, R.; Dewolf, C. E. Kinetic analysis of the ozone processing of an unsaturated organic monolayer as a model of an aerosol surface. *Phys. Chem. Chem. Phys.* **2007**, *9* (43), 5814–5821.

(50) Alebic-Juretic, A.; Cvitas, T.; Klasinc, L. Heterogeneous polycyclic aromatic hydrocarbon degradation with ozone on silica gel carrier. *Environ. Sci. Technol.* **1990**, *24* (1), 62–66.

(51) Martin, S. T. personal communication, 2008.

(52) Wu, C. H.; Salmeen, I.; Niki, H. Fluorescence Spectroscopic Study of Reactions Between Gaseous Ozone and Surface-Adsorbed Polycyclic Aromatic-Hydrocarbons. *Environ. Sci. Technol.* **1984**, *18* (8), 603–607.

(53) Michel, A. E.; Usher, C. R.; Grassian, V. H. Reactive uptake of ozone on mineral oxides and mineral dusts. *Atmos. Environ.* **2003**, *37* (23), 3201–3211.

(54) Usher, C. R.; Michel, A. E.; Stec, D.; Grassian, V. H. Laboratory studies of ozone uptake on processed mineral dust. *Atmos. Environ.* **2003**, *37* (38), 5337–5347.

(55) Vieceli, J.; Ma, O. L.; Tobias, D. J. Uptake and collision dynamics of gas phase ozone at unsaturated organic interfaces. *J. Phys. Chem. A* **2004**, *108* (27), 5806–5814.

(56) Rudich, Y.; Donahue, N. M.; Mentel, T. F. Aging of organic aerosol: Bridging the gap between laboratory and field studies. *Annu. Rev. Phys. Chem.* **2007**, *58*, 321–352.

JP8045802